Photodissociation dynamics of N_2O at 130 nm: The $N_2(A\,^3\Sigma_u^+, B\,^3\Pi_g) + O(^3P_{J=2,1,0})$ channels

Mark F. Witinski, Marivi Ortiz-Suárez, and H. Floyd Davis[a)]
Department of Chemistry and Chemical Biology, Baker Laboratory, Cornell University, Ithaca, New York 14853

(Received 29 October 2004; accepted 18 February 2005; published online 2 May 2005)

Oxygen Rydberg time-of-flight spectroscopy was used to study the vacuum ultraviolet photodissociation dynamics of N_2O near 130 nm. The $O(^3P_J)$ products were tagged by excitation to high-n Rydberg levels and subsequently field ionized at a detector. In agreement with previous work, we find that $O(^3P_J)$ formation following excitation to the repulsive N_2O $D(^1\Sigma^+)$ state produces the first two electronically excited states of the N_2 counterfragment, $N_2(A\,^3\Sigma_u^+)$ and $N_2(B\,^3\Pi_g)$. The $O(^3P_J)$ translational energy distribution reveals that the overall branching ratio between $N_2(A\,^3\Sigma_u^+)$ and $N_2(B\,^3\Pi_g)$ formation is approximately 1.0:1.0 for $J=1$ and 2, with slightly less $N_2(B\,^3\Pi_g)$ produced in coincidence with $O(^3P_0)$. The angular distributions were found to be independent of J and highly anisotropic, with $\beta=1.5\pm0.2$. © *2005 American Institute of Physics*. [DOI: 10.1063/1.1888578]

I. INTRODUCTION

Nitrous oxide (N_2O) is introduced into the atmosphere primarily through microbial action in soils. Once it is transported into the stratosphere, it absorbs strongly in the IR and is a much more potent greenhouse gas than CO_2 on a per molecule basis. It has been estimated that increasing the atmospheric N_2O concentration from 300 to 600 ppb (parts per 10^9) would cause the surface temperature of the Earth to increase by 0.3 K.[1] Nitrous oxide also plays a role in the balance of atmospheric ozone. Consequently, although N_2O is only a trace component of the atmosphere, doubling its concentration would result in a 12.5% depletion of O_3; the effect is even more pronounced in the presence of chlorofluorocarbons (CFC's).[2] The sources and sinks of atmospheric N_2O are therefore of interest to atmospheric scientists. One N_2O sink is photolysis in the vacuum ultraviolet (vuv). Excitation near 130 nm falls close to the peak of the strongly allowed transition from the ground $X(^1\Sigma^+)$ state to the repulsive $D(^1\Sigma^+)$ state.[3] The N_2O absorption cross section near 130 nm has been reported to be 7×10^{-17} cm^2 molec^{-1}.[4,5] A number of N_2+O photodissociation channels are energetically possible:

$$N_2O \rightarrow N_2(X\,^1\Sigma_g^+) + O(^3P), \quad (1)$$

$$N_2(X\,^1\Sigma_g^+) + O(^1D), \quad (2)$$

$$N_2(X\,^1\Sigma_g^+) + O(^1S), \quad (3)$$

$$N_2(A\,^3\Sigma_u^+) + O(^3P), \quad (4)$$

$$N_2(B\,^3\Pi_g) + O(^3P). \quad (5)$$

It has been demonstrated that channel (3) is dominant, with a quantum yield of 0.90 ± 0.05.[6,7] The remaining product yield is divided between channels (2), (4), and (5). Although channel (2) has been studied extensively around 193 nm,[8–12] it is relatively minor at 130 nm.

Reactions (4) and (5) are often probed indirectly through their contribution to NO γ band fluorescence from the reaction $N_2^*+NO\rightarrow N_2+NO^*$.[13,14] In the present study, we focused on reactions (4) and (5), which produce ground-state $O(^3P_J)$ atoms along with N_2 in electronically excited triplet states. Black *et al.* have estimated that $N_2(A\,^3\Sigma_u^+)$ formation, channel (4), may comprise 10% of the total product yield.[6] However, no estimate is available for channel (5), which is difficult to probe directly because $N_2(B\,^3\Pi_g)$ is quenched to $N_2(A\,^3\Sigma_u^+)$ by N_2O at a nearly gas kinetic rate,[15] and has a lifetime of only a few microseconds in the absence of quenching gas.[16]

Although there is no question that reactions (4) and (5) play a role in the vuv photodissociation of N_2O, little information is available concerning their dynamics. In 1971 Gilpin and Welge recorded time-of-flight spectra for products from N_2O photodissociation over three vuv wavelength regions.[17] While they were able to identify several metastable reaction products including $O(^1S)$, $O(^1D)$, $N(^2D)$, $N(^2P)$, and $N_2(A\,^3\Sigma_u)$, the energy resolution of the technique employed in their study was insufficient to provide insight into the products' angular distribution or into the level of vibrational excitation of the molecular fragments. We sought to obtain higher-resolution time-of-flight (TOF) spectra of $O(^3P_J)$ over a range of laboratory angles in order to understand the N_2O photodissociation process in greater detail.

The hydrogen Rydberg time-of-flight (HRTOF) method was originally developed by Schnieder *et al.*[18] In HRTOF, the H or D atom products from a reaction or photodissociation process are photoexcited to high-n Rydberg levels immediately following their formation in the interaction region,

[a)]Author to whom correspondence should be addressed. Electronic mail: hfd1@cornell.edu

and allowed to fly as neutrals to a detector where they are field ionized and counted. Some advantages of the method over other methods are the elimination of space-charge effects, high tagging efficiency, high velocity resolution, and high sensitivity.[19] We have recently developed oxygen Rydberg time-of-flight (ORTOF) in our laboratory as a means of extending the advantages of Rydberg tagging to processes generating ground-state, ^3P_J, oxygen atoms. Previously, we characterized this method through studies of the photodissociation of NO_2. We established that the lifetimes of oxygen atoms in intermediate Rydberg states ($n=19$–40) are sufficiently long to survive flights on the order of a few hundred microseconds without deliberate perturbation using external electric fields, which have been shown to extend Rydberg lifetimes by orders of magnitude.[20,21]

II. EXPERIMENT

The experiments were carried out using a fixed source, rotatable detector crossed molecular-beams apparatus.[19,22] The apparatus was recently upgraded by installing an oil-free turbomolecular pump and a dry pump to evacuate the main chamber. The base pressure of the scattering chamber was 1×10^{-6} Torr with the beam running. A molecular beam of N_2O was created by expanding 5-psi (gauge) neat N_2O (airgas 99.0%) from a piezoelectrically actuated pulsed valve (30 Hz). The N_2O beam was generated in a separately pumped chamber and collimated by a skimmer (Precision Instruments Inc.) before crossing the lasers in the main chamber about 8 cm away from the nozzle orifice.

The vuv radiation used for photolysis and product tagging was generated by resonance-enhanced four-wave mixing ($\omega_{\text{vuv}}=2\omega_R-\omega_T$) in a krypton gas cell.[23] The wavelength of the frequency-doubled dye laser (ω_R) was fixed to the two-photon resonance transition to the $5p[1/2]_0$ level of Kr near 212 nm, and that of the other dye laser (ω_T), operating near 580 nm, was varied to generate tunable vuv light near 130 nm. The exact wavelength of the photolysis light ranged from 130.27 nm for $O(^3P_2)$ to 130.60 nm for $O(^3P_0)$. The laser powers used in these experiments were as follows: $P(\omega_R)=0.5$ mJ; $P(\omega_T)=10$ mJ; and $P(\text{Rydberg})=4$ mJ. The ω_R and ω_T laser beams were combined using a dielectric mirror and focused by an achromatic doublet ($f=30$ cm) into the gas cell. The generated vuv light then passed through a MgF_2 lens ($f=20$ cm) into the main chamber where it crossed the molecular beam 4.5 cm away from the detector entrance aperture. The vuv radiation was linearly polarized, and its wavelength was tuned to the $^3S_1\leftarrow{}^3P_J$ transition of oxygen. Excitation of $O(^3S_1)$ atoms to $n=19$ was accomplished using the doubled output of a third dye laser operating near 305 nm (Rydberg Laser). All three dye lasers (Lambda Physik Scanmate 2) were pumped by a single Continuum Powerlite 9030 Nd:YAG (yttrium aluminum garnet) laser; their optical paths were carefully adjusted for spatial and temporal overlaps.

The "tagged" O atoms flew 34 cm through a field-free region, and were field ionized (2300 V/cm) and counted using a microchannel plate (Galileo). The ion signal was amplified by an EG&G VT120 preamplifier; TOF spectra were recorded by a Stanford Research Systems SR 430 multichannel scaler. A small dc voltage (+30 V) was applied to a thin-wire mesh (Precision Electroforming, 90% transmission) placed just in front of the multichannel plate (MCP) in the detector. This served to repel any ions that may have been produced in the main chamber from unintended processes such as multiphoton ionization.

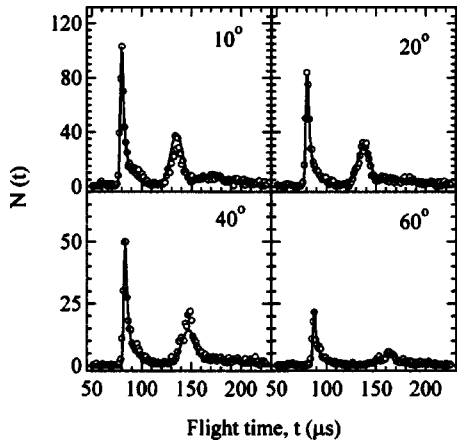

FIG. 1. Time-of-flight spectra at indicated laboratory angles relative to the plane containing the molecular beam and the vuv laser.

The product angular distribution for the reaction was measured in two different ways. With the vuv polarization fixed along the molecular-beam axis, the MCP detector was rotated in the plane of the N_2O beam, and the TOF spectra were recorded over a range of laboratory angles. We also obtained the angular distribution by rotating the photolysis polarization angle with respect to the molecular beam, and monitoring the ORTOF signal at a fixed detector angle. This was done by inserting a double Fresnel rhomb into the path of the 580-nm tunable dye laser and rotating it from 0° to 200°. Since the polarization of ω_T determines the polarization of the vuv,[24,25] by rotating the 580-nm polarization (measured to be >99% polarized), we rotated the probe polarization as well. In order to ensure that rotating the ω_T laser did not affect the laser alignment, $O(^3P_2)$ was generated by 212-nm photodissociation of SO_2 and probed by ORTOF. The signal level in that experiment was found to be independent of rhomb angle. Consequently, the strong variation in the ORTOF signal observed in the N_2O experiments as the rhomb was rotated must result from photofragment anisotropy.

III. RESULTS AND DISCUSSION

Figure 1 shows the TOF spectra (open circles) at four different laboratory angles for $O(^3P_2)$. The fast and slow peaks observed in the TOF spectra clearly correspond to the formation of $N_2(A\,^3\Sigma_u^+)$ and $N_2(B\,^3\Pi_g)$, respectively. The solid line in each graph is the fit generated using a forward convolution program. The program took as input a translational energy distribution, $P(E)$, the photofragment anisotropy parameter,[26] β, and experimental parameters including the beam spatial width, beam velocity spread, detector distance from the interaction region, and width of detector apertures. The program then convoluted over these parameters

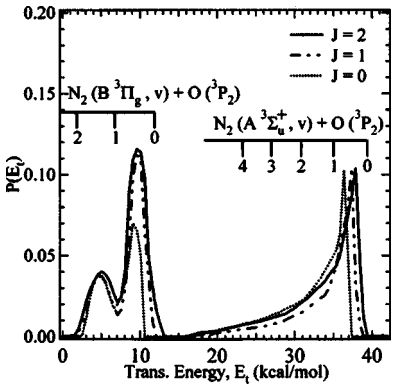

FIG. 2. O atom center-of-mass translational energy distributions for $O(^3P_{J=2,1,0})$. The maximum energies for the formation of $N_2(A\,^3\Sigma_u^+, B\,^3\Pi_g)$ in different vibrational levels are indicated for $O(^3P_2)$.

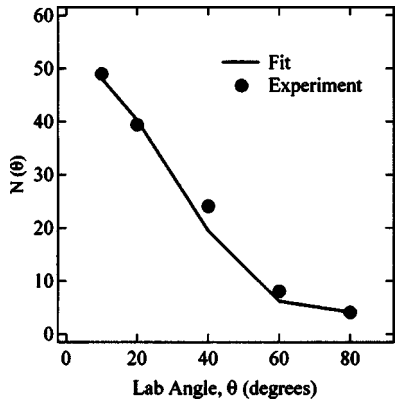

FIG. 3. The experimental laboratory angular distribution, $N(\theta)$, along with the simulation using $P(E)$ and β was shown.

to generate simulated TOF spectra. The $P(E)$ and β parameters were iteratively adjusted until the simulated spectra agreed with the experimental ones.

The translational energy resolution of the apparatus using ORTOF was checked in a separate series of experiments involving the 130.2-nm photodissociation of O_2. At this wavelength, both the $O(^3P)+O(^1D)$ and 2 $O(^3P)$ channels are formed. The two narrow peaks in the TOF spectra were fitted using the forward convolution program using the known apparatus function, measured beam velocity distribution and the known thermodynamic values for the two photodissociation channels. The only adjustable parameters were the width of the kinetic-energy distributions, $P(E)$, for each channel, which were found to have full width at half maximums of approximately 0.2 kcal/mol.

A. Translational energy distribution

The available translational energy (E_t) is given by

$$E_t = E_{h\nu} - D_0(N_2\text{–}O) - E_{INT}(N_2) - E_{INT}(O). \tag{6}$$

As ω_T is varied in order to probe different $O(^3P_J)$ states, both $E_{h\nu}$ and $E_{INT}(O)$ are changed. Consequently, the $P(E)$ used to fit $O(^3P_1)$ is shifted from that used to fit $O(^3P_2)$ by twice the difference in the ω_T. This is illustrated in Fig. 2, in which all three $P(E)$'s are plotted together. Integrating the two product manifolds that comprise each $P(E)$, we obtain a branching ratio for $N_2(A\,^3\Sigma_u^+):N_2(B\,^3\Pi_g)$ formation of 1.0:1.0 for $O(^3P_2)$, 1.0:1.0 for $O(^3P_1)$, and 1.0:0.7 for $O(^3P_0)$, indicating that some correlation between the internal energy of the two fragments exists. Specifically, $O(^3P_J)$ products with the highest degree of internal energy $(J=0)$ are more likely to be correlated with $N_2(A\,^3\Sigma_u^+)$.

As illustrated in Fig. 2, the structure in the $P(E)$ at energies below 13 kcal/mol is clearly due to the formation of $N_2(B\,^3\Pi_g)$ in $v=0$ and 1. From the $P(E)$, the ratio between $v=0$ and $v=1$ formation is approximately 2:1 The total available energy is only slightly above the threshold for the formation of $N_2(B\,^3\Pi_g)$ in $v=2$. No evidence was seen for this channel.

We were not able to resolve individual vibrational levels of the $N_2(A\,^3\Sigma_u)$ counterfragment. Since some rotational excitation may be imparted to N_2 if N_2O bends during dissociation, it is not possible to determine from our data the $N_2(A\,^3\Sigma_u)$ vibrational distribution. However, the contribution from $O(^3P_2)+N_2$ with E_{trans} greater than 35 kcal/mol indicates that for the $O(^3P_2)$ channel, at least 49% of the $N_2(A\,^3\Sigma_u^+)$ is in $v=0$.

B. Angular distributions

Figure 3 shows the experimental laboratoty angular distribution measured by rotating the detector, together with the simulated angular distribution for $O(^3P_2)$. The anisotropy parameter, β, is defined with respect to the laboratory angular distribution, $N(\theta)$, where θ is the angle between the polarization of the photolysis laser and the direction of product recoil:

$$N(\theta) = 1 + \beta P_2(\cos\theta), \tag{7}$$

where

$$P_2(\cos\theta) = (3\cos^2\theta - 1)/2. \tag{8}$$

The range of β is $-1 \leqslant \beta \leqslant 2$. In order to obtain the solid lines shown in Figs. 1 and 3, $\beta=1.5$ was input into the forward convolution program. We found that a β value of 1.5 ± 0.3 for all three spin-orbit levels of oxygen provided the best simulation of laboratory angular distribution data.

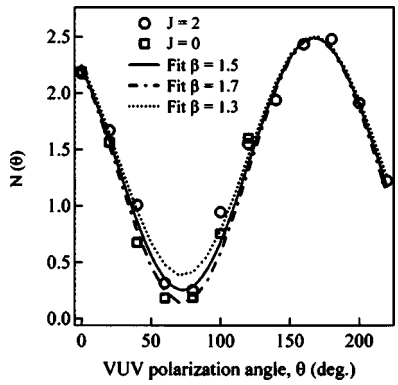

FIG. 4. Experimental signal levels for $O(^3P_2)$ (circles) and $O(^3P_0)$ (open squares) as a function of vuv polarization angle. $\theta=0°$ corresponds to vuv polarization along the molecular-beam axis. The fits were generated from Eq. (7) for a range of β parameters. $\beta=1.5$ (solid line) gives the best fit to the experimental data for both spin-orbit levels.

TABLE I. Summary of measurements for the three oxygen spin-orbit levels produced from N_2O photodissociation at 130 nm.

	$^3P_2$	$^3P_1$	$^3P_0$
$\%O(^3P_J)$	50±5	35±5	15±5
$N_2(A\,^3\Sigma_u^+):N_2(B\,^3\Pi_g)$	1.0 : 1.0 (± 0.1)	1.0 : 1.0 (±0.1)	1.0 : 1.0 (±.0.1)
β	1.5±0.2	1.5±0.2	1.5±0.2

A more sensitive measurement of the photofragment angular distribution involved a separate series of experiments, in which TOF spectra were recorded at a constant laboratory detector angle with the vuv polarization rotated to various angles. Since the $N_2(A\,^3\Sigma_u^+)$ and $N_2(B\,^3\Pi_g)$ contributions are well separated from one another, we first determined the integrated laser polarization angular distributions for each product channel separately. We found that they were the same for both channels to within the uncertainty of the measurement, so we integrated the whole TOF range to determine an overall angular distribution for the $O(^3P_J)$ product channel. Figure 4 shows the signal level for $O(^3P_2)$ and $O(^3P_0)$ as a function of vuv polarization angle, with the detector held at 20° with respect to the molecular-beam axis. These points were fitted to the expression in Eq. (7), where a phase offset was added to θ to convert the fits from the center-of-mass (CM) frame to the laboratory frame. We then varied β until the fit matched the experimental angular distribution. The figure shows the N (θ) distributions for β=1.7, 1.5, 1.3. The data for both $O(^3P_2)$ and $O(^3P_0)$ are best fitted with β=1.5, confirming the value generated by the forward convolution program in the rotating detector experiments. These fits are quite sensitive to β, allowing us to narrow our confidence interval to ±0.2. We observed no correlation between β and oxygen spin-orbit level, J. In the accompanying paper, Lambert *et al.* report small differences in the angular distributions as a function of N_2 and $O(^3P_{J=2,1,0})$ internal energy. The product angular distributions for N_2O photodissociation producing $O(^3P_2)$ was found to be independent of power for each of the three laser beams, indicating that saturation effects were not operative under our experimental conditions. Because photolysis and Rydberg tagging are accomplished using the same vuv pulse at 130 nm, it was not possible in our experiment to vary the relative polarization of the pump and probe lasers. Therefore, a small degree of alignment of $O(^3P_1)$ or $O(^3P_2)$ would probably be undetectable in our experiment.

C. Dissociation mechanism

In Table I, we summarize our measurements for each spin-orbit state of oxygen, including the overall J level branching ratio, the $N_2(A\,^3\Sigma_u^+):N_2(B\,^3\Pi_g)$ branching ratio, and β. In determining the spin-orbit branching ratio, we assumed that the absorption cross section of N_2O between 130.26 and 130.60 nm is constant and that all J's have the same oscillator strength for the $^3S_1 \leftarrow {}^3P_J$ transition. Within the error bars, our measured spin-orbit branching ratio of 5:3.5:1.5 is consistent with the 5:3:1 branching ratio expected for a statistical process.

The potential-energy surfaces for N_2O excited states in the range of 0–13 eV have been calculated.[27,28] The continuum from 120 to 140 nm is known to correspond to excitation to the repulsive $D(^1\Sigma^+)$ state, with 130.2 being very close to the peak of the absorption band. The $D(^1\Sigma^+)$ state correlates adiabatically with $N_2(X\,^1\Sigma_g^+)+O(^1S)$. However, as noted by Hopper, this adiabatic dissociation involves a two-electron transition, $2\pi^3 4\pi \rightarrow 9\sigma^2\pi^2$.[28] The $N_2(A\,^3\Sigma_u^+)+O(^3P)$ and $N_2(B\,^3\Pi_g)+O(^3P)$ product states correlate to several different excited N_2O levels in both a linear $C_{\infty v}$ and bent C_s geometry.[28] In a $C_{\infty v}$ configuration, $N_2(A\,^3\Sigma_u^+)$ may be produced either by direct dissociation from a repulsive $^3\Pi$ state, or from a $^1\Sigma^-$ state. On the other hand, $N_2(B\,^3\Pi_g)+O(^3P)$ correlates in $C_{\infty v}$ symmetry to N_2O states of $^3\Delta$ or $^3\Sigma$ symmetry. Since intersystem crossing of $N_2O(D^1\Sigma^+)$ to triplet excited levels should not play an important role in this fast dissociation process, the mechanism likely involves interactions between N_2O bent (C_s) states. As excited N_2O bends, the initially prepared $D(^1\Sigma^+)$ state transforms into states of A' symmetry. As noted long ago by Chutjian and Sega1,[27] a higher-lying-linear state of $^1\Pi$ symmetry, which correlates to $N_2(A\,^3\Sigma_u^+)+O(^3P)$, splits upon bending into the states of both A' and A'' symmetries. Indeed, the quenching of $N_2(A\,^3\Sigma_u^+)+O(^3P)$ is known to be rather efficient, and produces $N_2(X\,^1\Sigma_g^+)+O(^1S)$, likely via bent states of N_2O having A' symmetry.[29] Since dissociation from the initially prepared repulsive linear $D(^1\Sigma^+)$ state is expected to be fast, our observation that β is slightly reduced from the limiting value of 2.0 is likely due to some bending as N_2O dissociates.

This work was part of a cooperative effort between our group and the Houston group here at Cornell, to fully characterize the dynamics of N_2O dissociation at 130 nm. They have recently completed an extensive study of this system using photofragment ion imaging,[30] and their conclusions for the $N_2(A\,^3\Sigma_u^+, B\,^3\Pi_g)+O(^3P_{J=2,1,0})$ channels are in qualitative agreement with ours. They have also obtained angular and product energy distributions for channels (2) and (3) as well as for certain NO+N product channels.

ACKNOWLEDGMENTS

This research was supported by the Office of Science, U. S. Department of Energy under Grant No. DE-FG02-00ER15095. The authors acknowledge valuable discussions with H. M. Lambert and P. L. Houston.

[1] J. S. Levine, *The Photochemistry of Atmospheres* (Academic, Orlando, 1985).
[2] R. P. Wayne, *Chemistry of Atmospheres*, 2nd ed. (Oxford University Press, New York, 1991).

[3]J. B. Nee, J. C. Yang, P. C. Lee, X. Y. Wang, and C. T. Kuo, J. Phys. B **31**, 5175 (1998).
[4]M. Zelikoff, K. Watanabe, and E. C. Y. Inn, J. Chem. Phys. **21**, 1643 (1953).
[5]J. B. Nee, J. C. Yang, P. C. Lee, X. Y. Wang, and C. T. Kuo, Chin. J. Phys. (Taipei) **37**, 172 (1999).
[6]G. Black, R. L. Sharpless, T. G. Slanger, and D. C. Lorents, J. Chem. Phys. **62**, 4266 (1975).
[7]E. J. Stone, G. M. Lawrence, and C. E. Fairchild, J. Chem. Phys. **65**, 5083 (1976).
[8]Y. Matsumi and A. M. S. Chowdhury, J. Chem. Phys. **104**, 7036 (1996).
[9]S. Nishida, K. Takahashi, Y. Matsumi, N. Taniguchi, and S. Hayashida, J. Phys. Chem. A **108**, 2451 (2004).
[10]T. F. Hanisco and A. C. Kummel, J. Phys. Chem. **97**, 7242 (1993).
[11]D. W. Neyer, A. J. R. Hech, and D. W. Chandler, J. Chem. Phys. **110**, 3411 (1999).
[12]N. Balakrishnan, V. Kharchenko, and A. Dalgarno, J. Phys. Chem. A **103**, 3999 (1999).
[13]L. Schnieder, W. Meier, K. H. Welge, M. N. R. Ashfold, and C. M. Western, J. Chem. Phys. **92**, 7027 (1990).
[14]H. Okabe, J. Chem. Phys. **47**, 101 (1967).
[15]R. A. Young, G. Black, and T. G. Slanger, J. Chem. Phys. **50**, 303 (1969).
[16]M. Jeunehomme, J. Chem. Phys. **45**, 1805 (1966).
[17]R. Gilpin and K. H. Welge, J. Chem. Phys. **55**, 975 (1971).
[18]L. Schnieder, K. Seekamp-Rahn, E. Wrede, and K. H. Welge, J. Chem. Phys. **107**, 6175 (1997).
[19]C. Lin, M. F. Witinski, and H. F. Davis, J. Chem. Phys. **119**, 251 (2003).
[20]L. Y. Baranov, A. Held, H. L. Selzle, and E. W. Schlag, Chem. Phys. Lett. **291**, 311 (1998).
[21]A. Held, L. Y. Baranov, H. L. Selzle, and E. W. Schlag, Chem. Phys. Lett. **291**, 318 (1998).
[22]B. R. Strazisar, C. Lin, and H. F. Davis, Phys. Rev. Lett. **86**, 3997 (2001).
[23]J. P. Marangos, N. Shen, H. Ma, M. H. R. Hutchinson, and J. P. Connerade, J. Opt. Soc. Am. B **7**, 1254 (1990).
[24]K. Tsukiyama, M. Tsukakoshi, and T. Kasuya, Opt. Commun. **81**, 327 (1991).
[25]L. Museur, C. Olivero, D. Riedel, and M. C. Castex, Appl. Phys. B: Lasers Opt. **70**, 499 (2000).
[26]R. N. Zare, Mol. Photochem. **4**, 1 (1972); G. E. Busch and K. R. Wilson, J. Chem. Phys. **56**, 3626 (1972); **56**, 3638 (1972).
[27]A. Chutjian and G. A. Segal, J. Chem. Phys. **57**, 3069 (1972).
[28]D. G. Hopper, J. Chem. Phys. **80**, 4309 (1984).
[29]J. A. Meyer, D. W. Setster, and D. H. Stedmen, Astrophys. J. **157**, 1023 (1969).
[30]D. W. Chandler and P. L. Houston, J. Chem. Phys. **87**, 1445 (1987).